Ecotoxicology and Environmental Safety 286 (2024) 117255

Contents lists available at ScienceDirect

Ecotoxicology and Environmental Safety

journal homepage: www.elsevier.com/locate/ecoenv

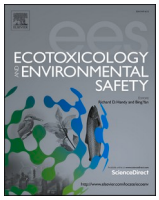

Differential sensitivity of hemocyte subpopulations (*Mytilus edulis*) to aged polyethylene terephthalate micro- and nanoplastic particles

Jenevieve Hara [a,b,*], Maaike Vercauteren [b], Sébastjen Schoenaers [c], Colin R. Janssen [b], Ronny Blust [a], Jana Asselman [b], Raewyn M. Town [a]

[a] ECOSPHERE, Department of Biology, University of Antwerp, Groenenborgerlaan 171, Antwerp 2020, Belgium
[b] Blue Growth Research Lab, Ghent University, Wetenschapspark 1, Ostend 8400, Belgium
[c] IMPRES, Department of Biology, University of Antwerp, Groenenborgerlaan 171, Antwerp 2020, Belgium

ARTICLE INFO

Edited by Professor Bing Yan

Keywords:
Aged PET, Hemocytes
In-vitro
Functional assays
Immunotoxicity
Flow cytometry

ABSTRACT

Bivalve hemocytes, particularly granulocytes and hyalinocytes, play a crucial role in cell-mediated immunity. However, their interactions with aged plastic particles, exhibiting altered properties that more closely resemble those in natural environments, remain largely underexplored. This study assesses the differential responses of hemocyte subpopulations *(Mytilus edulis)* to chemically aged polyethylene terephthalate (PET) microplastic (MPs) and nanoplastic (NPs) particles across multiple cellular effect endpoints. Particle characteristics were analyzed using Single Particle Extinction and Scattering, Raman Spectroscopy, Scanning Electron Microscopy, and Dynamic Light Scattering. In vitro experiments with aged PET MPs (1.9 μm) and NPs (0.68 μm) were conducted at three internally relevant concentrations: 10 (C1), 10^3 (C2), and 10^5 particles/mL (C3). Cellular responses were assessed by measuring lysosomal content stability, reactive oxygen species (ROS) production, cellular mortality, and morphological parameters using flow cytometry at 6, 12, 24, and 48 hours. Our findings provide mechanistic insights into the differential sensitivities of granulocytes and hyalinocytes to aged PET, influenced by particle size and concentration. Specifically, aged PET MPs and NPs induce distinct size and concentration-dependent patterns of lysosomal destabilization, coinciding with the loss of functional integrity. Elevated ROS levels were observed only in granulocytes and hyalinocytes exposed to high concentrations of aged PET NPs, underscoring the effects on oxidative stress. Both aged PET MPs and NPs induce significant increases in cellular mortality, particularly after 24 h of exposure at high concentrations. These findings reveal the complex cellular mechanisms underlying hemocyte functional impairment following exposure to aged PET particles under environmentally and biologically relevant conditions.

1. Introduction

Plastic pollution, particularly in the form of micro- and nanoplastic particles (MPs/NPs), is prevalent in the environment, raising concerns about its adverse effects on aquatic organisms (Liu et al., 2024). These particles mainly originate from two sources: the direct discharge of primary MPs into the environment and the degradation of larger plastic materials, resulting in the formation of secondary particles (Ali et al., 2024). While there is a growing body of research documenting various biological responses to plastic particle exposure, systematic analyses of effect endpoints at the cellular level remain limited (Prinz and Korez, 2020). Yet, this information is crucial for understanding the fundamental pathways and mechanisms of exposure and determining how MPs and NPs pose health risks (Sharifinia et al., 2020).

Innate immunity, the primary defense mechanism in invertebrates, is integral for overall functioning (Canesi and Procházková, 2014). It affects various biological aspects, including histopathology, bioenergetics, and susceptibility to infections, which can ultimately lead to mortality (Kataoka and Kashiwada, 2021). Invertebrate immune cells, particularly hemocytes of bivalve mollusks, play a crucial role in cell-mediated immunity and serve as valuable models for investigating particle-induced responses (Canesi and Procházková, 2014). Different subpopulations of hemocytes, such as granulocytes and hyalinocytes, exhibit distinct morphological and functional characteristics (Le Foll et al., 2010), including internal cell signaling pathways that regulate various cellular processes (Canesi et al., 2006). Granulocytes are the dominant cell type

* Correspoding author at: ECOSPHERE, Department of Biology, University of Antwerp, Groenenborgerlaan 171, Antwerp 2020, Belgium.
E-mail address: jenevieve.hara@uantwerpen.be (J. Hara).

https://doi.org/10.1016/j.ecoenv.2024.117255
Received 9 September 2024; Received in revised form 18 October 2024; Accepted 23 October 2024
Available online 26 October 2024

in the hemolymph of *Mytilus spp.*, characterized by high phagocytic activity and oxyradical production, whereas hyalinocytes have lower phagocytic ability (Le Foll et al., 2010). Phagocytosis, one of the critical immune defense functions of these specialized cells, regulates the internalization of particles (>0.5 μm in diameter), such as pathogens, apoptotic bodies, and other foreign materials (Rosales and Uribe-Querol, 2017). Phagocytosis typically occurs concomitantly with autophagy, a lysosome-based degradative pathway essential for maintaining cellular homeostasis (Gustafson et al., 2015). However, dysregulation of autophagy can compromise lysosomal stability, disrupt homeostasis, and lead to oxidative stress, inflammation, and mitochondrial dysfunction. These cellular disturbances can ultimately trigger cell death pathways, potentially resulting in adverse effects at the organismal level (Stern et al., 2012). Extensive literature has documented the effects of various particles, including metallic, ceramic, and polymeric nanoparticles, on cellular systems. These studies revealed that micro and nanoparticles can induce a range of cellular responses, from uptake and processing to adverse toxicological outcomes (Stern et al., 2012). The interactions of particles with cells and the resulting biological effects are significantly influenced by physicochemical properties, including particle size, shape, surface charge, and composition (Foroozandeh and Aziz, 2018). Despite the recognized capability of various particles, including plastic particles, to penetrate biological membranes and affect cellular mechanisms, significant gaps remain in understanding the systemic toxicity, particularly concerning the immune system (Sharifinia et al., 2020).

The intricate response pathways and regulatory networks governing cellular stress and death offer multiple targets for comprehensive toxicological studies (Simmons et al., 2009), taking into account various physicochemical properties. However, numerous studies have raised concerns regarding the environmental relevance of plastic particles employed in laboratory experiments (Karami, 2017). Previous studies investigating the effects of MPs and NPs have predominantly utilized polystyrene (PS) spheres or beads and often involve unrealistic exposure conditions (Ferreira et al., 2019), including simplified particle sizes, shapes, and concentrations that do not reflect real-world scenarios. This narrow focus limits the understanding of the broader impact of plastic pollution, as it overlooks the environmental relevance and potential toxicity of other polymers, such as polyethylene terephthalate (PET). For instance, PET is one of the most prevalent polymer types in the marine environment (Ashrafy et al., 2023) and is commonly ingested by filter-feeding organisms, particularly mussels (Pequeno et al., 2021; Qu et al., 2018). Studies have reported that ingested MPs accumulate in the hemolymph of mussels, with smaller particles (3.0 μm) being more abundant than larger ones (9.6 μm) and persisting in the circulatory system for over 48 days (Browne et al., 2008). Using concentrations that match those detected internally, such as in the hemolymph of mussels, is crucial for a more accurate assessment of biological responses.

Additionally, the aging and weathering of plastic particles introduce critical variables that significantly affect the interaction with biological systems (Lu et al., 2023). Through processes such as photodegradation, physical abrasion, and chemical degradation, aged and weathered particles acquire altered surface and physicochemical properties (He et al., 2023). These changes can potentially lead to heightened toxicological profiles compared to their pristine counterparts (Völkl et al., 2022). Modifications induced by particle aging, particularly in size, shape, and surface properties, can enhance particle-cell interactions, thereby influencing cellular uptake mechanisms and toxicity profiles (Foroozandeh and Aziz, 2018). Using aged particles is crucial to accurately reflect actual environmental conditions (Revel et al., 2021), where particles are rarely pristine and often undergo significant transformations before interacting with biological systems.

To address existing knowledge gaps, this study investigated the responses of hemocyte subpopulations to chemically aged polyethylene terephthalate micro- and nanoplastic particle exposure across multiple cellular effect endpoints. Specifically, hemocytes extracted from blue mussels (*Mytilus edulis*) were exposed to aged PET particles with two distinct size ranges and three concentrations, chosen to reflect both environmentally and biologically relevant conditions. Cellular responses (lysosomal content stability, reactive oxygen species (ROS) production, cellular mortality) and morphological parameters (cell size and complexity), were assessed using flow cytometry at various time points. By integrating responses related to particle size, concentration, and exposure time, this study provided insights into the critical cellular mechanisms underlying the effects of exposure to aged plastic particles.

2. Materials and methods

2.1. Characterization of the aged PET Micro- and nanoplastic particles

Aged polyethylene terephthalate (PET) MPs and NPs with irregular shapes and heterogeneous sizes were obtained through mechanical cryomilling and chemical aging. The primary stock suspensions with particles smaller than 5 μm were processed and provided by the Joint Research Centre (JRC) of the European Commission. To isolate the particles in the sub-micrometer range, the suspension was sonicated for 20 minutes, sedimented for 12 h, and filtered through a 1 μm membrane filter. The aging process for PET involved immersion in potassium hydroxide solution (KOH) combined with ultrasonic treatment, which induced the formation of polar COO^- groups resulting in enhanced particle hydrophilicity, as indicated by Sioen et al. (2024) for particles produced by the JRC. This method has been reported to yield surface modifications similar to those of naturally aged particles (von der Esch et al., 2020), highlighting the suitability of these particles as reference materials.

The polymer composition, size, shape, and concentration of the particles in the stock solution were confirmed using Raman spectroscopy (reference library Open Specy), scanning electron microscopy (SEM, Phenom™ ProX Desktop), and the single particle extinction and scattering (SPES, Classizer™ ONE) technique (Supplementary Figures A.1 – A.3 and Table A.1). Two different size ranges of aged PET were utilized: MPs with an average dimension of 1.9 μm (D_{10} = 0.6 μm; D_{50} = 1.4 μm and D_{90} = 3.1 μm) and NPs with an average dimension of 0.68 μm (D_{10} = 0.39 μm; D_{50} = 0.57 μm; and D_{90} = 1.1 μm). D10, D50, and D90 represent percentile values from the cumulative particle size distribution analyzed using SPES, indicating the size below which 10 %, 50 %, and 90 % of the particles are found (Supplementary Figure A.1, Panel A and B). Stock solutions contained 4.0×10^7 and 1.66×10^7 particles per mL (denoted as P/mL), respectively. Aged PET particles were suspended in Milli-Q water without surfactant. Secondary characterization of the aged PET MPs and NPs was conducted using Dynamic Light Scattering (DLS, Zetasizer Nanoseries, Malvern Instruments) at various time points (1 h, 24 h, and 48 h) to ensure particle stability under conditions adopted for the in-vitro exposure experiments (Supplementary Figure A.4).

2.2. Maintenance of the mussel culture

Adult mussels (*Mytilus edulis)* were collected from the Scheldt Estuary in Hoedekenskerke, Netherlands. Mussels were kept in a glass aquarium with artificial seawater (hw-Marinemix Professional), equipped with portable aeration (Eheim Air Pump 400) and mechanical-biological filtration (Eheim Biopower 200) systems. The temperature was maintained at 15 ± 0.4°C with a photoperiod (12:12 h). The mussels were fed daily with microalgae suspension (*Tetraselmis suecica*, Tetraprime S Proviron), with the water inflow interrupted for 2 hours during feeding. Water was replaced by 50 % daily, and quality parameters (pH (8.08 ± 0.05), salinity (30.9 ± 0.5 ‰), dissolved oxygen (8.12 ± 0.21 mg/L), ammonia (0.25 mg/L, nitrite (<0.3 mg/L), and nitrate (12.5 mg/L) were monitored using Hach HQ40D meters and Tetra test kits. Prior to experimental procedures, the mussels were acclimatized and depurated under laboratory conditions for a minimum period of three weeks. No mortality was observed under these conditions.

2.3. Hemolymph extraction and cell culture preparation

A total of 80–100 adult mussels, with shell lengths of 4–6 cm, were selected for hemolymph extraction and cell culture following established protocols (Katsumiti et al., 2017). Mussels were anesthetized for 30 minutes using a filtered (100 nm, Millipore) and sterilized 0.3 M magnesium chloride ($MgCl_2$) solution within a laminar airflow cabinet (Spetec). Hemolymph was extracted from the posterior abductor muscle using a sterile 2 mL syringe (Injekt) with a 23 G needle (Terumo Neolus). The extracted hemolymph was pooled, filtered through a 70 μm cell strainer (Greiner) to eliminate impurities and aggregates, and then diluted at a 9:1 ratio in an anti-aggregation solution (171 mM NaCl; 0.2 M Tris; 0.15 % v/v HCl 1 N; 24 mM EDTA, with reported $>$ 95 % viability (Katsumiti et al., 2017)). The concentration and purity of the cell suspension were verified using a hemocytometer (MUHWA Scientific, Neubauer), microscope (Nikon, Eclipse LV100N POL), and flow cytometer (BD Biosciences). Cell suspensions were then seeded into pre-labeled 24-well glass bottom microplates (Greiner Bio-one) and maintained in filtered (0.2 μm; Millipore) culture media (Basal Medium Eagle (BME), Sigma Aldrich) supplemented with L-Glutamine and an antibacterial agent (0.001 % Gentamicin). Strict aseptic techniques were maintained throughout the procedure to prevent contamination.

2.4. In-vitro exposure experiments

The experiment employed a full factorial design, comprising two aged PET particle size ranges and three concentrations: 10 P/mL (C1); 10^3 P/mL (C2); and 10^5 P/mL (C3). These chosen particle properties align with the reported concentration ranges and represent the most abundant size classes of accumulated plastic particles in the hemolymph of mussels (Browne et al., 2008). Initially, working solutions (10^6 P/mL) of MPs and NPs were separately prepared in culture media and diluted to obtain the desired exposure concentrations. Suspensions were systematically sonicated for 20 minutes to ensure uniform particle dispersion before use.

The in-vitro exposure experiment was carried out using pooled hemocytes suspended in culture media with a cell concentration of 1×10^6 cells/mL and incubated at 15°C. This selected cell concentration has been effectively applied in previous in vitro experiments with various test particles (Katsumiti et al., 2021), compounds (Bouki et al., 2013; Katsumiti et al., 2017), and microbial challenges (Tanguy et al., 2018). Each treatment was conducted in triplicate and cells were incubated under stable culture conditions for 6 h, 12 h, 24 h, and 48 h. Treatments included a pure culture medium as the negative control (NC) and a culture medium containing varying concentrations of aged PET MPs and NPs. Adequate positive control treatments were included for each measured parameter (see below). At each sample time, cells were collected from the culture wells and washed twice with phosphate-buffered saline (PBS) before analysis.

2.5. Assessment of cellular endpoints

Cellular endpoints were measured to assess the effect of aged PET MPs or NPs exposure on hemocyte subpopulations using fluorescent labeling and flow cytometry with BD™ LSR II (BD Biosciences).

2.5.1. Cellular morphology

Morphological changes in hemocytes were detected using the side scatter (SSC) and forward scatter (FSC) detectors of the flow cytometer, which are parameters based on cell size and internal complexity (Sendra et al., 2020). Data on morphological parameters are expressed in arbitrary units (A.U.).

2.5.2. Lysosomal stability

Lysosomal stability was assessed using the LysoTracker™ Blue DND-22 (Invitrogen), a cell-permeable dye applicable for labeling and tracing acidic organelles such as lysosomes (Wang et al., 2019). Hydrogen peroxide (H_2O_2, 100 μM) was used as a positive control to induce cellular stress conditions impacting lysosomal stability (Brunk et al., 1995). Cell samples were suspended in PBS with 75 nM LysoTracker™ and incubated in the dark at 15°C for 1 h. Fluorescence was measured with the flow cytometer at excitation and emission wavelengths of 373 nm and 422 nm, respectively. Intracellular lysosomal content is expressed as the mean geometric fluorescence in hemocyte subpopulations relative to the negative control (set to 100 %).

2.5.3. Reactive oxygen species (ROS) production

Intracellular ROS production was assessed using the 5-(and-6)-chloromethyl-2′,7′-dichlorodihydrofluorescein diacetate acetyl ester (CM-H_2DCFDA, Invitrogen), dissolved in dimethylsulfoxide (DMSO) (Yang and Wang, 2022). As a positive control, oxidative activity was induced using H_2O_2 at a sub-lethal concentration of 100 μM (Brunk et al., 1995; Sendra et al., 2020). Cell samples were suspended in PBS with 10 μM CM-H_2DCFDA and incubated in the dark at 15°C for 1 h. DCF green fluorescence was measured with the FITC signal detector (FL1) of the flow cytometer. ROS production is expressed as the mean geometric fluorescence in hemocyte subpopulations relative to the negative control (set to 100 %).

2.5.4. Cellular mortality

Cellular mortality was assessed using Propidium Iodide (PI; Abcam), following the manufacturer's protocol with modifications (Wang et al., 2019). As positive controls, cells were incubated with Cadmium Chloride ($CdCl_2$, 800 μM) to induce cellular death (PC CT) (Olabarrieta et al., 2001). Additionally, sonication for 1 h was included as a second non-chemical positive control (PC ST). Cell samples were suspended in 500 μl of binding buffer with 5 μl of PI (50 μg/mL), and incubated in the dark at 15°C for 5–10 min. Fluorescence was measured with excitation and emission wavelengths of 535 nm and 617 nm, respectively. Data were expressed as the percentage (%) of non-viable cells relative to the total cell count per hemocyte subpopulation.

2.6. Flow cytometry analyses

Flow cytometry, a fluorescence-based technology, was used to identify and characterize hemocyte subpopulations, such as granulocytes and hyalinocytes. Analysis was performed using a BD™ LSR II flow cytometer (BD Biosciences) equipped with 488 nm (blue), 633 nm (red), 405 nm (violet), and 355 nm (UV) lasers. Hemocyte subpopulations were detected using SSC and FSC parameters, based on cell size and complexity. Initially, unexposed hemocytes served as a baseline to establish the normal SSC and FSC profiles, ensuring measurements were unaffected by potential interference from plastic particles. A gating technique using the SSC vs. FSC dot plots was then employed to distinguish the sub-population of interest. A total number of 10,000 cells was analyzed in each sample replicates. Regular calibration was performed using calibration beads to ensure accurate parameter measurement throughout the experiment. Data were processed using FACSDiva™ Software (Version 5.0) and FlowJo (Version 10.9.0).

2.7. Statistical analysis

The normal distribution of the data was assessed using the Shapiro-Wilk test. The effects of particle size and concentration of aged PET MPs and NPs were analyzed by two-way analysis of variance (ANOVA). If interactions between factors were identified, significant effects of particle size, concentration, and time were further examined either using a one-way ANOVA or the non-parametric Kruskal-Wallis test, based on normality assessment of the data. Pairwise comparisons were performed with Tukey's HSD post-hoc test (Wang et al., 2019). Differences were considered significant at $P < 0.05$. All analysis was conducted using GraphPad Prism (Version 10.1.2). The graphical abstract was created

with BioRender.com.

3. Results

The responses of hemocyte subpopulations to various concentrations of aged PET MPs and NPs across multiple cellular effect endpoints are described in detail in the following sections and summarized in Supplementary Table A.2.

3.1. Cellular morphology (Size and Complexity)

Granulocytes and hyalinocytes exposed to increasing concentrations of aged PET MPs and NPs showed no significant changes in cell size and complexity (Figs. 1 - 2 and Supplementary Table A.2) over 6, 12, 24, and 48 h.

3.2. Lysosomal stability

Analysis of lysosomal content in hemocytes after exposure to different concentrations of aged PET MPs and NPs revealed distinct size-specific and concentration-dependent patterns of destabilization (Fig. 3 and Supplementary Table A.2).

Granulocytes exposed to aged PET MPs showed a size-specific increase in lysosomal content at 12 h and 48 h of exposure. Particularly, concentration-dependent increases of 43.2 % and 45.5 % at C2 ($p = 0.045$) and C3 ($p = 0.030$) compared with the control were observed after 48 h (Fig. 3, panel A). Among the NP-treated groups, only the highest aged PET NP concentration (C3) induced a significant increase in lysosomal content at 24 h, by 78.7 % and 76.5 % compared to the control ($p = 0.020$) and C1 ($p = 0.024$). Interestingly, a relatively lower lysosomal content was observed in all NP-treated groups after 48 h, though not significantly different from the concurrent control.

Hyalinocytes exhibited a variable lysosomal response to aged PET particle exposure (Fig. 3, panel B). In MP-treated groups, a concentration-dependent elevation in lysosomal content was observed only at 48 hours, with MP C2 ($p = 0.015$) and C3 ($p = 0.026$) inducing increases of 54.3 % and 50.9 %. While in hyalinocytes exposed to NPs, no significant changes in lysosomal content were observed across all time points. Similar trends of relatively lower lysosomal content were evident after 48 h of NP exposure, though not statistically significant.

As the positive control, H_2O_2 induced an abrupt increase in lysosomal content in both hemocyte subpopulations ($p < 0.05$), followed by a stabilization over time (Supplementary Figure A.5, Panel A and B).

3.3. Oxidative activity

ROS levels in granulocytes exposed to various aged PET MP concentrations did not show significant differences across all time points (Fig. 4, panel A). In contrast, exposure to aged PET NPs resulted in a significant increase in ROS production only at the highest concentration (C3) at 24 h, with a 45.5 % increase compared to the control ($p = 0.047$).

Similarly, hyalinocytes exposed to various MP concentrations did not exhibit significant differences in ROS production compared to the control (Fig. 4, panel B). However, exposure to NPs resulted in a significant increase in ROS production of 184 % only at the highest concentration (C3) at 24 h ($p = 0.009$).

The positive control with H_2O_2 induced significant changes ($p < 0.05$) in ROS levels in granulocytes only at 6 h, while no significant changes were observed in hyalinocytes (Supplementary Figure A.5, Panel C and D).

3.4. Cellular mortality

The results demonstrated a significant adverse effect of aged PET exposure on hemocyte mortality, with a concentration- and time-dependent increase in PI-positive cells (Fig. 5 and Supplementary Table A.2). Specifically, aged PET MP concentrations C2 and C3 significantly increased granulocyte mortality to 15.9 % ($p = 0.021$) and 16.5 % ($p = 0.007$), respectively, compared with the control (11.6 %). These correspond to percentage increases of approximately 37.8 % and 42.9 % after 24 h of exposure. No significant concentration-dependent changes in mortality were observed 48 h post-exposure to MPs, though C2 exhibited the highest rate among all tested concentrations (Fig. 5, panel A). Among the NP-treated groups, only C3 induced a significant increase in granulocyte mortality to 17.6 % ($p = 0.016$) compared with the control (13.0 %) at 24 h, corresponding to a 35.0 % increase. After 48 h exposure, NP C3 remained elevated although not statistically significant.

In hyalinocytes (Fig. 5, panel B), only the highest MP concentration (C3) significantly increased mortality to 13.0 % compared with the control (8.42 %) at 24 h ($p = 0.039$), corresponding to a 54.5 % increase compared to the control cells. Although there were increments in mortality rates at higher concentrations after 48 h, no significant concentration-dependent differences between MPs and NPs were observed in hyalinocytes.

The positive controls, PC ST (sonication treatment, $p < 0.0001$ in both hemocyte subpopulations) and PC CT (chemical treatment, $p < 0.0001$ in granulocytes and $p < 0.05$ in hyalinocytes), exhibited a high number of PI-positive cells, particularly after 24 h. This indicates high mortality rates and validates the sensitivity of the assay (Supplementary Figure A.6, Panel A and B).

4. Discussion

Hemocytes serve as the first line of defense against contaminants in bivalves, making them a crucial model for evaluating the effects of MPs and NPs on immune functions (Canesi and Procházková, 2014). This study aimed to elucidate how these particles, particularly aged PET, affect hemocyte subpopulations through the analysis of multiple cellular effect endpoints. Key findings revealed differential sensitivities of hemocyte subpopulations, influenced by particle size, concentration, and exposure time.

4.1. Morphological characterization of hemocyte subpopulations

Flow cytometry enabled the morphological differentiation of hemocyte subpopulations and quantitative assessment of cellular markers (Bajgelman, 2019). This technique effectively distinguished two distinct hemocyte subpopulations: granulocytes, characterized by larger cell size and higher internal complexity, and hyalinocytes, with smaller size and lower complexity (Le Foll et al., 2010). Exposure to increasing concentrations of aged PET MPs and NPs did not induce significant changes in cell size or complexity for both subpopulations over time. In contrast, exposure of hemocytes to different concentrations of PS NPs (100 nm and 1 μm) resulted in significant changes in cell size, while no corresponding changes in cell complexity were observed (Sendra et al., 2020). In another cell type, exposure to 50 nm amine-modified polystyrene (NH_2-PS-NPs, 50 μg/mL or 7.28×10^{11} P/mL converted concentration in Supplementary Table A.3) did not alter cell size but increased complexity over time, likely due to enhanced vacuolization (Wang et al., 2013).

4.2. Lysosomal destabilization in response to Aged PET exposure

This study reveals distinct patterns of lysosomal destabilization influenced by particle size and concentration. As observed, exposure to aged PET MPs resulted in progressive fluctuations in lysosomal content across hemocyte subpopulations at higher concentrations. Aged NP exposure significantly increased lysosomal content in granulocytes at the highest tested concentration, followed by a subsequent reduction after prolonged NP exposure, suggesting potential alterations in

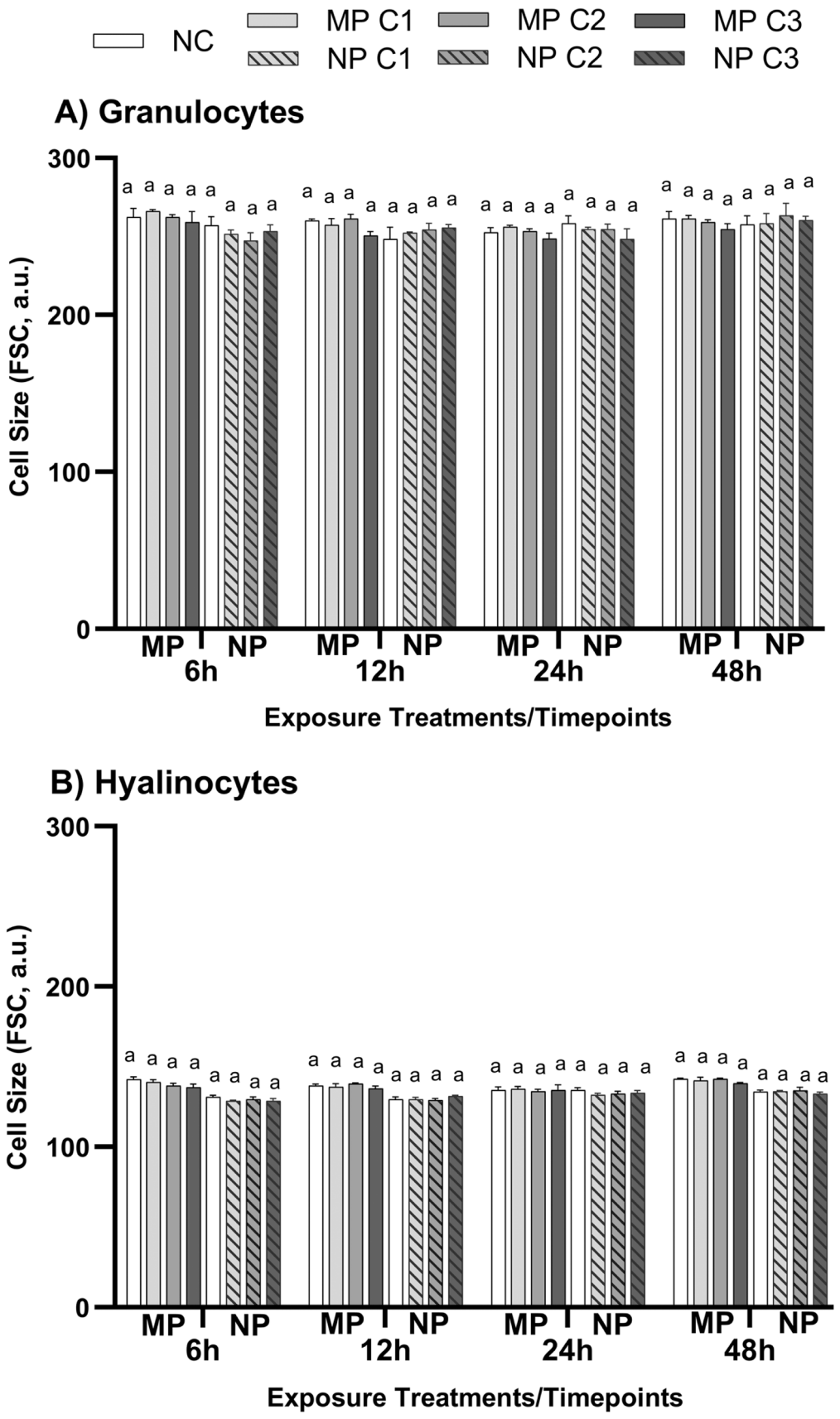

Fig. 1. Cell size (FSC, a.u.) in (A) granulocytes and (B) hyalinocytes exposed to different concentrations of aged PET microplastic (MP) and nanoplastic (NP) particles (C1:10 P/mL; C2: 10^3 P/mL; C3: 10^5 P/mL) over 6, 12, 24, and 48 h. Data are expressed as mean ± SD (n=3). Different lower-case letters at each fixed MP or NP treatment denote significant differences among concentrations at each time point ($P < 0.05$). Asterisks indicate significant differences between particle sizes at each concentration per time point (*$P < 0.05$; ** $P \leq 0.01$; *** $P \leq 0.001$).

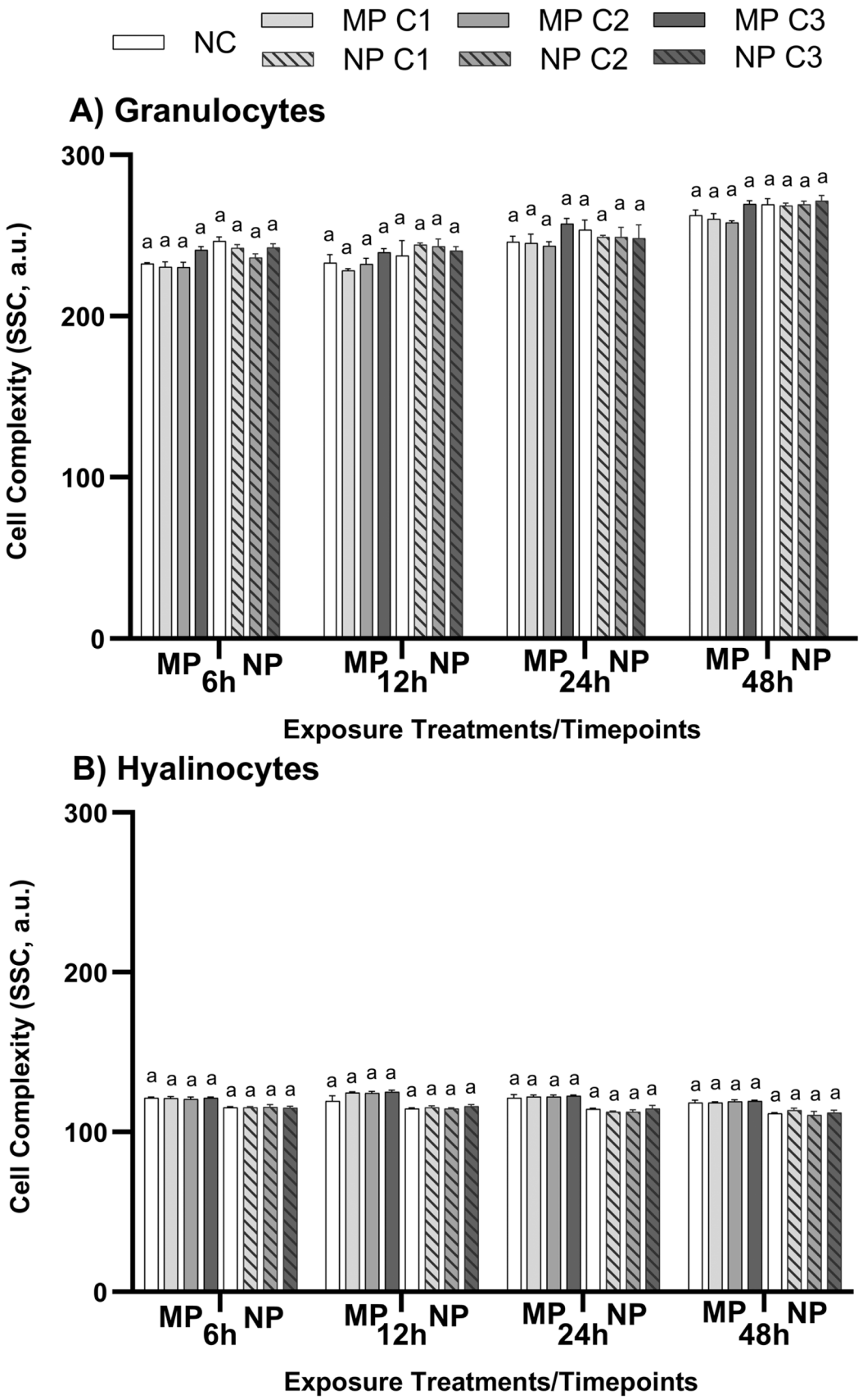

Fig. 2. Cell complexity (SSC, a.u.) in (A) granulocytes and (B) hyalinocytes exposed to different concentrations of aged PET microplastic (MP) and nanoplastic (NP) particles (C1:10 P/mL; C2: 10^3 P/mL; C3: 10^5 P/mL) over 6, 12, 24, and 48 h. Data are expressed as mean ± SD (n=3). Different lower-case letters at each fixed MP or NP treatment denote significant differences among concentrations at each time point ($P < 0.05$). Asterisks indicate significant differences between particle sizes at each concentration per time point (*$P < 0.05$; ** $P \leq 0.01$; *** $P \leq 0.001$).

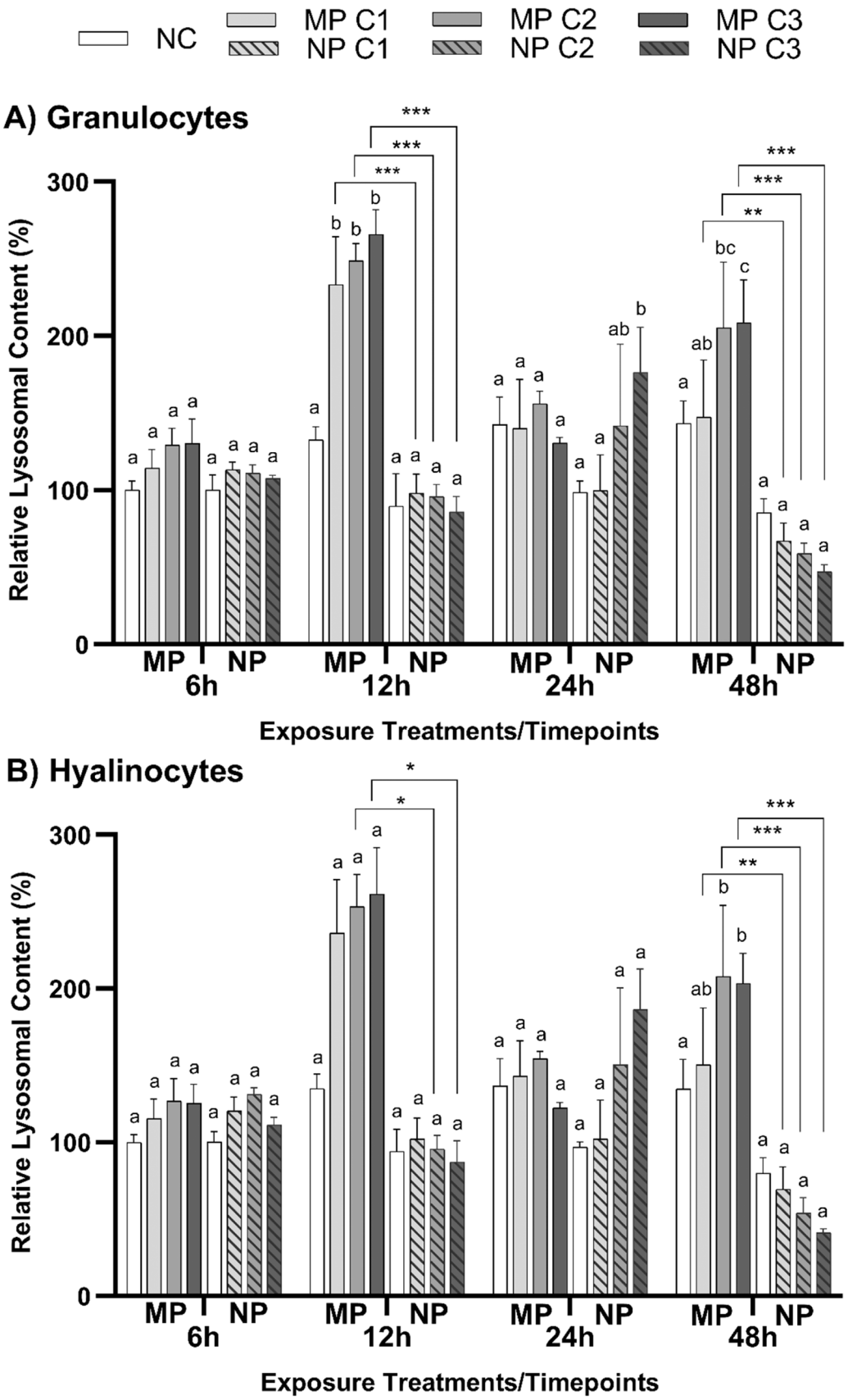

Fig. 3. Relative lysosomal content in (A) granulocytes and (B) hyalinocytes exposed to different concentrations of aged PET microplastic (MP) and nanoplastic (NP) particles (C1:10 P/mL; C2: 10^3 P/mL; C3: 10^5 P/mL) over 6, 12, 24, and 48 h. Data are expressed as mean ± SD (n=3). Different lower-case letters at each fixed MP or NP treatment denote significant differences among concentrations at each time point ($P < 0.05$). Asterisks indicate significant differences between particle sizes at each concentration per time point (*$P < 0.05$; ** $P \leq 0.01$; *** $P \leq 0.001$).

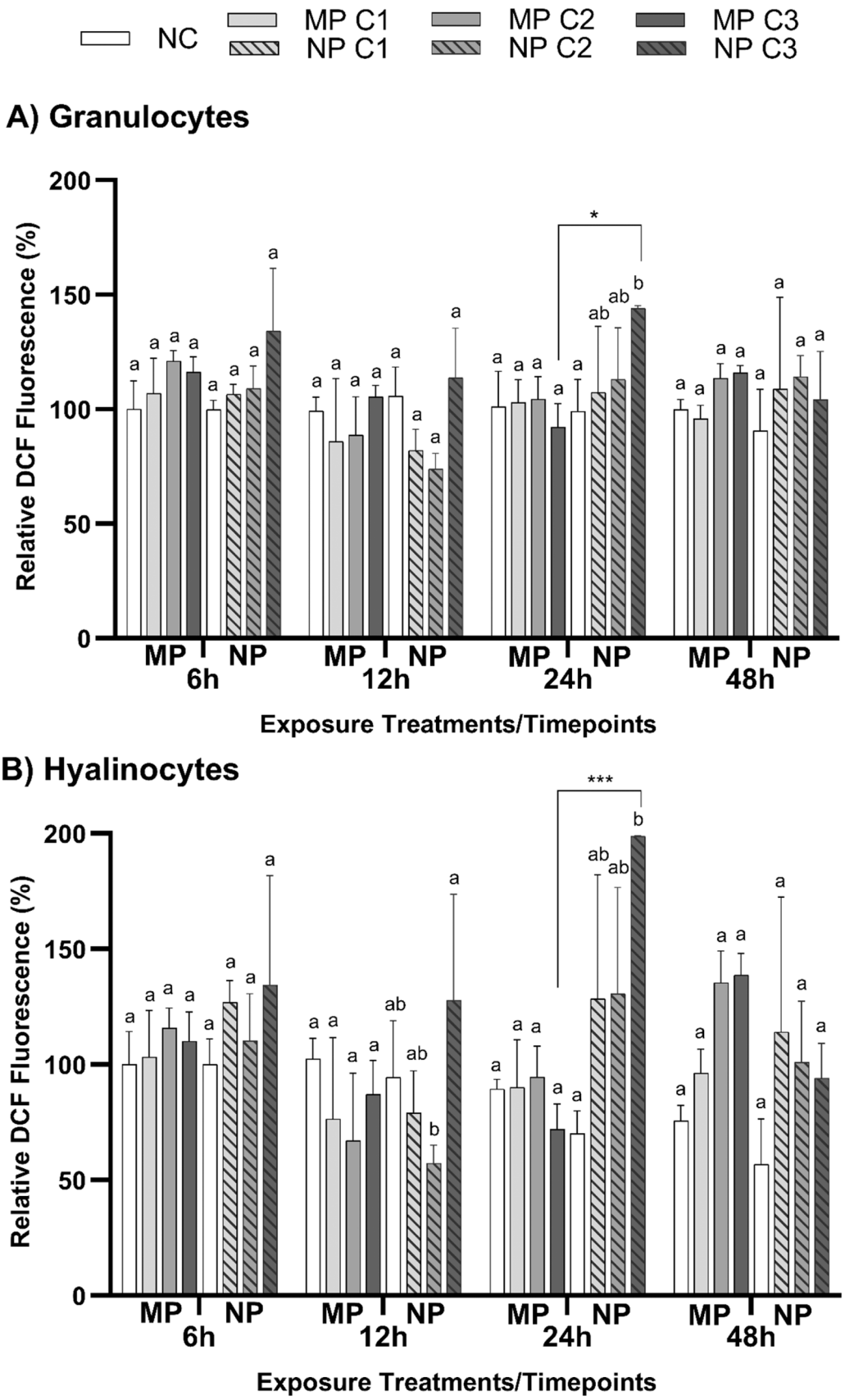

Fig. 4. Relative reactive oxygen species (ROS) production in (A) granulocytes and (B) hyalinocytes exposed to different concentrations of aged PET microplastic (MP) and nanoplastic (NP) particles (C1:10 P/mL; C2: 10^3 P/mL; C3: 10^5 P/mL) over 6, 12, 24, and 48 h. Data are expressed as mean ± SD (n=3). Different lowercase letters at each fixed MP or NP treatment denote significant differences among concentrations at each time point ($P < 0.05$). Asterisks indicate significant differences between particle sizes at each concentration per time point (*$P < 0.05$; ** $P \leq 0.01$; *** $P \leq 0.001$).

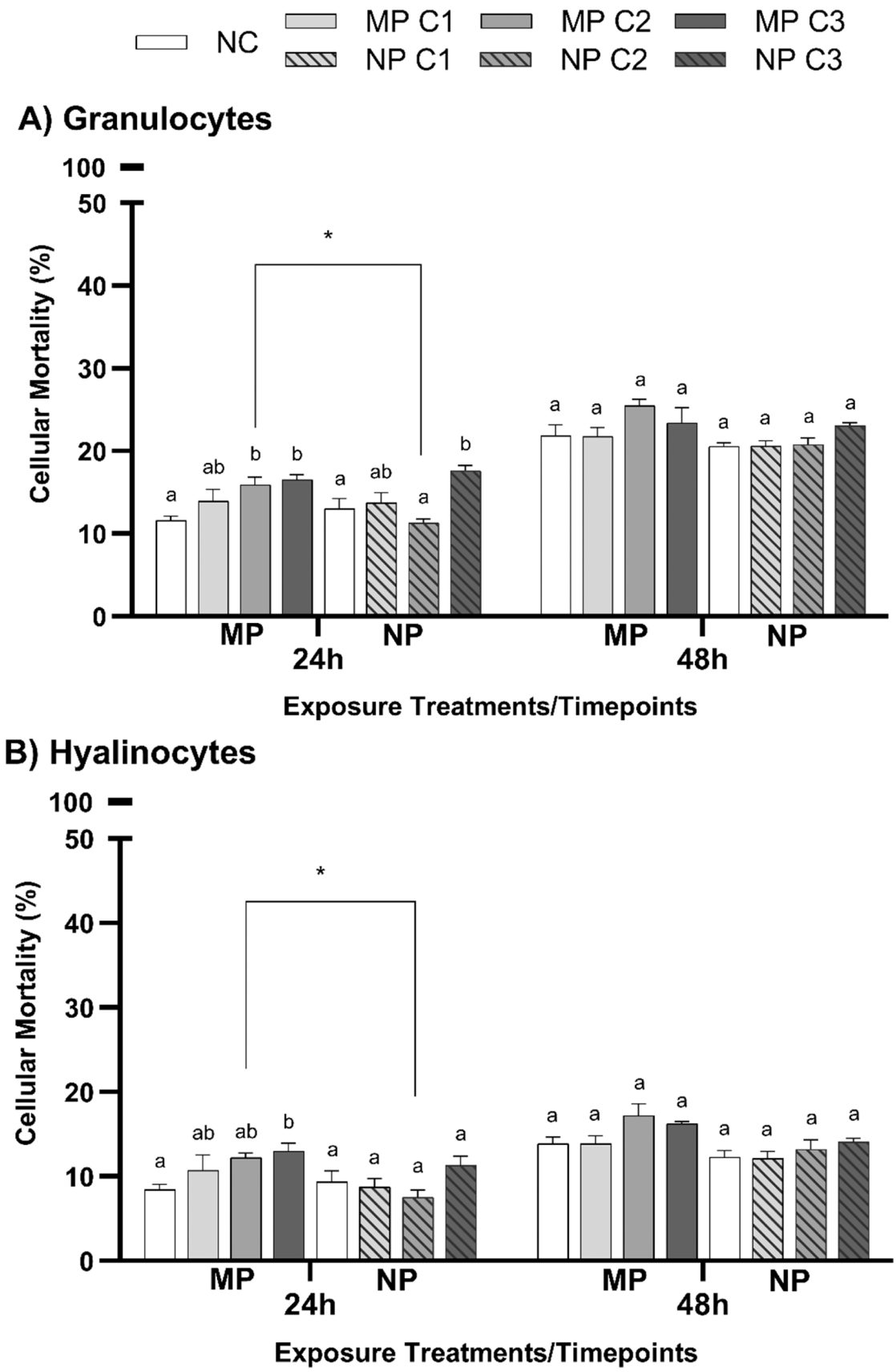

Fig. 5. Cellular mortality in (A) granulocytes and (B) hyalinocytes exposed to different concentrations of aged PET microplastic (MP) and nanoplastic (NP) particles (C1:10 P/mL; C2: 10^3 P/mL; C3: 10^5 P/mL) over 24 h and 48 h. Data are expressed as mean ± SD (n=3). Different lower-case letters at each fixed MP or NP treatment denote significant differences among concentrations at each time point ($P < 0.05$). Asterisks indicate significant differences between particle sizes at each concentration per time point (*$P < 0.05$; ** $P \leq 0.01$; *** $P \leq 0.001$).

lysosomal membrane integrity. For this analysis, the acidotropic dye LysoTracker was used to label acidic cellular compartments, primarily lysosomes. Fluctuations in LysoTracker fluorescence intensity indicate changes in lysosomal pH, membrane permeabilization, and overall functionality (Gaudioso et al., 2022; Oberle et al., 2010). Similar patterns were observed in embryonic zebrafish fibroblast cell lines exposed to different sizes of NH_2-PS-NPs beads. Larger-sized particles (1000 nm, 20 μg/mL or 3.64 $\times 10^7$ P/mL) have been reported to induce acidification of the lysosomal compartment, whereas smaller-sized NPs (100 nm, 20 μg/mL or 3.64 $\times 10^{10}$ P/mL) exhibited a decrease in fluorescence within 3–9 h post-exposure, both coinciding with the loss of lysosomal integrity (Yang and Wang, 2022). This reduction can be attributed to the leakage of proteolytic lysosomal enzymes into the cytosol, causing alkalization and lysosomal dysfunction (Lunov et al., 2011).

Additionally, the observed changes in lysosomal stability suggest that hemocytes undergo activation of phagocytic machinery in response to particle exposure. The activation of phagocytic pathways refers to the cellular process where highly specialized phagocytes (Le Foll et al., 2010), such as granulocytes, recognize and internalize extracellular particles. Due to their active role in the intracellular digestion of foreign material, granulocytes have been reported to exhibit a substantially higher lysosomal content than hyalinocytes (Sendra et al., 2020). Engulfed particles are typically processed within the lysosomal compartment, where phagosomes fuse with lysosomes to form phagolysosomes for degradation (Rosales and Uribe-Querol, 2017). Several studies have confirmed particle localization within lysosomes. For instance, in mussel hemocytes exposed to 0.5 μm and 4.5 μm PS at 10^8 P/mL and 10^9 P/mL, particles were found inside membrane-bound phagolysosomal vesicles (Katsumiti et al., 2021). Similarly, in mouse macrophages, PET NPs (191.6 nm) were reported to exhibit higher uptake than other tested particles (160 nm and 1.30 μm LDPE, and 1.85 μm PET), accumulating in lysosomes and the cytosol but not in mitochondria or other organelles (Deng et al., 2022). This indicates a preferential uptake and irreversible accumulation of polymeric particles within lysosomal compartments, with no clear evidence of particle degradation or exit processes (Salvati et al., 2011). Another study demonstrated that PET NPs remain stable in a simulated lysosomal environment, even over extended periods of up to two months, highlighting their intracellular biopersistence and long-term stability (Magrì et al., 2018).

4.3. Oxidative stress induced by aged PET NPs

The marked increase in ROS production observed only with aged PET NPs, particularly at the highest concentration tested in this study, indicates a significant size-specific and concentration-dependent effect on oxidative stress. Oxidative stress occurs when ROS production exceeds the capacity of antioxidant defenses, including enzymes like glutathione peroxidase, catalase, and superoxide dismutase. This imbalance can abnormally activate cellular signaling pathways (Chaitanya et al., 2016). Previous studies have extensively reported heightened ROS production induced by various MPs and NPs as a key initiating event, potentially leading to irreparable oxidative damage. This size-dependent effect, particularly pronounced in aged PET NPs, is attributed to the increased surface-to-mass ratio, which enhances their ability to interact with and penetrate cellular components (Hu and Palić, 2020). Similarly, polypropylene (PP) fragments aged through UV irradiation have been reported to induce nearly twice the ROS generation in hemocytes compared to pristine fragments, emphasizing the influence of particle aging on oxidative stress processes (Chelomin et al., 2024). Other carbon-based (C60 fullerenes), silicon-based (SiO_2), and metal oxide (TiO_2) NPs exhibited varying extents and time courses of ROS production in hemocytes, with SiO_2 reported to induce the highest concentration-dependent increase (Canesi et al., 2010). In RAW 264.7 macrophage cells, exposure to PET NPs (50–250 nm) with irregular shapes and sizes also led to a significant increase in intracellular ROS, but with no concentration-dependent correlation (Aguilar-Guzmán et al., 2022). These findings highlight that while particle size and concentration are crucial factors influencing ROS generation potential, their effects can vary across various cell types.

4.4. Mechanisms of hemocyte dysfunction induced by aged PET exposure

The significant increase in cellular mortality observed after 24 h of in-vitro exposure highlights the concentration-dependent cytotoxicity of aged PET particles. The adverse effects were more pronounced at high concentrations, particularly in granulocytes, as shown by the increase in PI-positive cells. PI, which binds to DNA, only penetrates cells with compromised membranes, emitting red fluorescence that identifies dead cells regardless of the mechanism of cell death (Crowley et al., 2016). Similarly, a dose-dependent increase in hemocyte mortality was observed after 24 h of in-vitro exposure to environmental NPs and MPs, mainly composed of polyethylene (PE) with sizes ranging from 1 – 1.2 μm and 1.2 – 300 μm (Roman et al., 2023). Exposure to 50 nm PS-NH_2 significantly increased the percentage of hemocytes undergoing necrotic processes, detected after a shorter exposure duration of 45 min at the highest tested concentration (50 μg/mL or 7.28 $\times 10^{11}$ P/mL) (Canesi et al., 2015). In another study with virgin PS (1 μm), granulocytes were identified as the most affected hemocyte subpopulation, with a comparatively higher percentage of non-viable cells (36.3 %) after 3 h of exposure (10 mg/L or 1.82 $\times 10^7$) (Sendra et al., 2020). Exposure to environmental NPs and MPs (LDPE, PET, and PS) in mouse macrophages did not significantly induce cellular mortality, suggesting these cells can adapt to chronic exposure despite initial signs of dysfunction (Deng et al., 2022).

The findings of this study provide insights into the complex cellular mechanisms underlying hemocyte functional impairment following exposure to aged particles under environmentally and biologically relevant conditions. Initially, cellular defense mechanisms, involving lysosomal and phagocytic pathways, attempt to mitigate the cytotoxic effects, but these defenses become overwhelmed over time. This distinct induction of cellular dysfunction aligns with recent studies, such as those on embryonic zebrafish fibroblast cell lines, where NH_2-PS particles of different sizes induced varying lysosomal changes and ROS production, leading to different cell death mechanisms (Yang and Wang, 2022).

As a recognized mechanism of particle toxicity, lysosomal dysfunctions induced by particle exposure play a crucial role in modulating cellular death signaling pathways (Stern et al., 2012). Previous studies have highlighted the ‘proton sponge’ effect, where particles, especially those containing amine groups, absorb protons in the acidic lysosomal environment. This process leads to ion and water influx, causing lysosomal swelling and rupture and contributing to the induction of cytotoxicity (Nel et al., 2009). For instance, a time-resolved study demonstrated that the accumulation of NH_2-PS-NPs initiated these processes, ultimately inducing mitochondrial damage and apoptosis (Wang et al., 2013). Specifically, partial lysosomal membrane permeabilization (LMP) is linked to ROS induction and apoptosis, whereas massive LMP causes cytosolic acidification and necrosis (Stern et al., 2012). The effect on lysosomal functionality is not unique to polymeric particles, as negatively charged silica particles have also been linked to lysosomal injury and the release of lysosomal enzymes, which induce apoptosis in alveolar macrophages (Thibodeau et al., 2004). Thus, incorporating assays for lysosomal function into the biological screening system is essential for detecting pathological alterations associated with particle exposure (Xia et al., 2008).

4.5. Influence of weathering on particle-induced cellular responses

Moreover, the cellular effects of weathered particles can be linked to the accumulation of reactive groups and radicals on the surface. For instance, weathered polystyrene particles (2 μm at 150 μg/mL or 3.41 $\times 10^7$ P/mL) have been observed to induce significantly higher ROS

levels in murine macrophages compared to pristine counterparts (Völkl et al., 2022). Conversely, in THP-1 macrophages exposed to particles with size ranges of approximately 90 μm at 20,000 P/mL, pristine MPs induced higher cellular ROS levels compared to weathered polypropylene and polystyrene. As previously indicated, weathered particles have a higher binding affinity for serum proteins than pristine ones. These proteins act as ROS scavengers, neutralizing free radicals and thereby reducing the overall ROS generation potential of the weathered MPs (Jeon et al., 2021). Nevertheless, as another recognized mechanism of particle-induced systemic toxicity, the extent of ROS generation and its impact on cellular health are influenced by particle properties, cell types, and exposure conditions (Hu and Palić, 2020).

Previous studies indicated that the cytotoxic effects of plastic particle exposure could be partly attributed to leachable components, such as surfactants and residual monomers (Völkl et al., 2022). To minimize the compounding influence of leachable components, a surfactant-free particle stock suspension was used in this study. Although PET typically contains plasticizers such as di-n-propyl phthalate, diethyl phthalate (DEP), and di-n-butyl phthalate (DBP), it demonstrates enhanced stability compared to polymers with a carbon-only backbone (PP, PE, PS, and PVC) (Do et al., 2022). Extensive studies have shown that PET microplastics have slow rates of additive leaching and contain the lowest additive levels among tested polymers under environmental conditions (Bridson et al., 2023). Biological assessments in mussel hemocytes, particularly focusing on lysosomal membrane stability (LMS), revealed no significant impact from PET leachates. This suggests that the observed cytotoxicity is primarily driven by the particles themselves rather than by any leachate components (Capolupo et al., 2020).

5. Conclusions and future directions

This study provides mechanistic insights into how aged PET MPs and NPs affect both granulocytes and hyalinocytes by analyzing multiple cellular endpoints. Key findings reveal differential sensitivity among hemocyte subpopulations, influenced by particle size and concentration. Specifically, aged PET MPs and NPs induce distinct size-specific and concentration-dependent patterns of destabilization, both coinciding with the loss of functional integrity. Elevated ROS levels were observed only with aged PET NPs at high concentrations, underscoring effects on oxidative stress. Both aged PET MPs and NPs induce significant increases in cellular mortality, particularly after 24 hours of exposure at high concentrations. The findings underscore the complex cellular mechanisms that impact hemocyte functional integrity following exposure to aged PET particles under environmentally and biologically relevant conditions.

It is important to note that evaluating the potential exacerbation of cellular responses under chronic exposure conditions is constrained by the limited longevity of primary hemocyte cultures. No permanent cell line from marine invertebrates has been established yet, as these cells typically stop dividing and exhibit cellular quiescence within 24–72 hours post-isolation (Rinkevich, 2011). In studying contaminants such as nanomaterials, it has been noted that outcomes from short-term in vitro experiments with isolated cells may not reliably reflect the potential effects observed at the organism level in vivo (Canesi et al., 2012). This limitation underscores the necessity of employing relevant exposure conditions for in vitro testing, ensuring that particle concentrations align with those detected internally in organisms. Previous studies have demonstrated that cytotoxicity was induced in hemocytes following both in vitro and in vivo exposure (Luo and Wang, 2022; Roman et al., 2023). These findings suggest that when properly designed, in vitro approaches can serve as reliable predictors of in vivo outcomes (Barrick et al., 2018), given that primary cells offer relevant transcriptomic and proteomic profiles, as well as physiological functions and responses (Gaudioso et al., 2022). Moreover, in vitro models are invaluable tools for generating extensive data and providing fast, reliable assessment of the ecotoxic properties of plastic particles (Revel et al., 2021). Given the morphological and functional similarity to mammalian immune cells, bivalve hemocytes can serve as a useful model for comparative regulatory studies (Canesi and Procházková, 2014).

While this study provides crucial mechanistic insights, the intrinsic toxicity mechanisms of a broader range of environmentally relevant plastic particle properties alongside the need for in-vivo validation, highlight areas for future research. Subsequent studies should focus on elucidating the mechanisms of particle uptake and intracellular trafficking routes to better assess ensuing toxicity profiles (Foroozandeh and Aziz, 2018). With the potential of hemocytes to exhibit heightened bioreactivity and intracellular accumulation, a thorough understanding of the impacts on cellular organelles and processes is imperative. Holotomography, as a cutting-edge imaging technique, provides high-resolution, label-free, and three-dimensional visualization capabilities for assessing both intracellular localization and dynamic cellular responses (Yoon et al., 2015). Such a holistic approach will provide a comprehensive understanding of the potential systemic effects of environmentally relevant MPs and NPs on both cellular and organismal health.

CRediT authorship contribution statement

Colin R Janssen: Supervision, Funding acquisition. **Ronny Blust:** Supervision, Funding acquisition. **Maaike Vercauteren:** Writing – review & editing, Methodology, Formal analysis, Conceptualization. **Sébastjen Schoenaers:** Writing – review & editing, Methodology, Formal analysis. **Jenevieve Hara:** Writing – review & editing, Writing – original draft, Methodology, Investigation, Formal analysis, Data curation, Conceptualization. **Jana Asselman:** Writing – review & editing, Supervision, Funding acquisition. **Raewyn M Town:** Writing – review & editing, Supervision, Methodology, Funding acquisition.

Declaration of Competing Interest

The authors declare the following financial interests/personal relationships which may be considered as potential competing interests:

Raewyn M. Town reports a relationship with Ecotoxicology and Environmental Safety that includes: board membership. Co-author is a member of the International Editorial Board of Ecotoxicology and Environmental Safety - R.M.T. If there are other authors, they declare that they have no known competing financial interests or personal relationships that could have appeared to influence the work reported in this paper.

Acknowledgments

Jenevieve Hara is supported by the RESPONSE project, funded under the Joint Action Ecological Aspects of Microplastics of JPI Oceans (B2/20E/P1/ RESPONSE “Toward a risk-based assessment of microplastic pollution in marine ecosystems”) and Research Foundation - Flanders (FWO) (G053320N “Towards ecological risk assessment of nanoplastics: dynamic considerations). Maaike Vercauteren is funded by the Special Research Fund of Ghent University (Grant BOF21/PDO/081). Test particles and the primary characterization were supplied by the Joint Research Centre (JRC), with the support of John Seghers, Håkan Emteborg, and Claudia Cella. We also appreciate the assistance of Gethrie Oraño with the in-vitro experiment.

Appendix A. Supporting information

Supplementary data associated with this article can be found in the online version at doi:10.1016/j.ecoenv.2024.117255.

Data availability

Data will be made available on request.

References

Aguilar-Guzmán, J.C., Bejtka, K., Fontana, M., Valsami-Jones, E., Villezcas, A.M., Vazquez-Duhalt, R., Rodríguez-Hernández, A.G., 2022. Polyethylene terephthalate nanoparticles effect on RAW 264.7 macrophage cells. Micro Nanoplastics 2 (1). https://doi.org/10.1186/s43591-022-00027-1.

Ali, N., Khan, M.H., Ali, M., Sidra, Ahmad, S., Khan, A., Nabi, G., Ali, F., Bououdina, M., Kyzas, G.Z., 2024. Insight into microplastics in the aquatic ecosystem: properties, sources, threats and mitigation strategies. Sci. Total Environ. 913. https://doi.org/10.1016/j.scitotenv.2023.169489.

Ashrafy, A., Liza, A.A., Islam, M.N., Billah, M.M., Arafat, S.T., Rahman, M.M., Rahman, S. M., 2023. Microplastics pollution: a brief review of its source and abundance in different aquatic ecosystems. J. Hazard. Mater. Adv. 9. https://doi.org/10.1016/j.hazadv.2022.100215.

Bajgelman, M.C., 2019. Principles and Applications of Flow Cytometry. In Data Processing Handbook for Complex Biological Data Sources. Elsevier, pp. 119–124. https://doi.org/10.1016/B978-0-12-816548-5.00008-3.

Barrick, A., Guillet, C., Mouneyrac, C., Châtel, A., 2018. Investigating the establishment of primary cultures of hemocytes from Mytilus edulis. Cytotechnology 70 (4), 1205–1220. https://doi.org/10.1007/s10616-018-0212-x.

Bouki, E., Dimitriadis, V.K., Kaloyianni, M., Dailianis, S., 2013. Antioxidant and pro-oxidant challenge of tannic acid in mussel hemocytes exposed to cadmium. Mar. Environ. Res. 85, 13–20. https://doi.org/10.1016/j.marenvres.2012.12.005.

Bridson, J.H., Abbel, R., Smith, D.A., Northcott, G.L., Gaw, S., 2023. Release of additives and non-intentionally added substances from microplastics under environmentally relevant conditions. Environ. Adv. 12. https://doi.org/10.1016/j.envadv.2023.100359.

Browne, M.A., Dissanayake, A., Galloway, T.S., Lowe, D.M., Thompson, R.C., 2008. Ingested microscopic plastic translocates to the circulatory system of the mussel, Mytilus edulis (L.). Environ. Sci. Technol. 42 (13), 5026–5031. https://doi.org/10.1021/es800249a.

Brunk, U.T., Zhang, H., Dalen, H., llinger, K., 1995. Exposure of cells to nonlethal concentrations of hydrogen peroxide induces degeneration-repair mechanisms involving lysosomal destabilization. Free Radic. Biol. Med. 19 (6), 813–822. https://doi.org/10.1016/0891-5849(95)02001-q.

Canesi, L., Ciacci, C., Pruzzo, C., 2006. Cell signaling in the immune response of mussel hemocytes. Invertebr. Surviv. J. 3 (1), 40–49.

Canesi, L., Ciacci, C., Bergami, E., Monopoli, M.P., Dawson, K.A., Papa, S., Canonico, B., Corsi, I., 2015. Evidence for immunomodulation and apoptotic processes induced by cationic polystyrene nanoparticles in the hemocytes of the marine bivalve Mytilus. Mar. Environ. Res. 111, 34–40. https://doi.org/10.1016/j.marenvres.2015.06.008.

Canesi, L., Ciacci, C., Fabbri, R., Marcomini, A., Pojana, G., Gallo, G., 2012. Bivalve molluscs as a unique target group for nanoparticle toxicity. Mar. Environ. Res. 76, 16–21. https://doi.org/10.1016/j.marenvres.2011.06.005.

Canesi, L., Ciacci, C., Vallotto, D., Gallo, G., Marcomini, A., Pojana, G., 2010. In vitro effects of suspensions of selected nanoparticles (C60 fullerene, TiO2, SiO2) on Mytilus hemocytes. Aquat. Toxicol. 96 (2), 151–158. https://doi.org/10.1016/j.aquatox.2009.10.017.

Canesi, L., Procházková, P., 2014. The Invertebrate Immune System as a Model for Investigating the Environmental Impact of Nanoparticles. In Nanoparticles and the Immune System. Academic Press, pp. 91–112. https://doi.org/10.1016/B978-0-12-408085-0.00007-8.

Capolupo, M., Sørensen, L., Jayasena, K.D.R., Booth, A.M., Fabbri, E., 2020. Chemical composition and ecotoxicity of plastic and car tire rubber leachates to aquatic organisms. Water Res. 169, 115270. https://doi.org/10.1016/j.watres.2019.115270.

Chaitanya, R.K., Shashank, K., Sridevi, P., 2016. Oxidative Stress in Invertebrate Systems. In Free Radicals and Diseases. InTech. https://doi.org/10.5772/64573.

Chelomin, V.P., Istomina, A.A., Mazur, A.A., Slobodskova, V.V., Zhukovskaya, A.F., Dovzhenko, N.V., 2024. New insights into the mechanisms of toxicity of aging microplastics. Toxics 12 (10), 726. https://doi.org/10.3390/toxics12100726.

Crowley, L.C., Scott, A.P., Marfell, B.J., Boughaba, J.A., Chojnowski, G., Waterhouse, N. J., 2016. Measuring cell death by propidium iodide uptake and flow cytometry. Cold Spring Harb. Protoc. 2016 (7), 647–651. https://doi.org/10.1101/pdb.prot087163.

Deng, J., Ibrahim, M.S., Tan, L.Y., Yeo, X.Y., Lee, Y.A., Park, S.J., Wüstefeld, T., Park, J. W., Jung, S., Cho, N.J., 2022. Microplastics released from food containers can suppress lysosomal activity in mouse macrophages. J. Hazard. Mater. 435, 128980. https://doi.org/10.1016/j.jhazmat.2022.128980.

Do, A.T.N., Ha, Y., Kwon, J.H., 2022. Leaching of microplastic-associated additives in aquatic environments: a critical review. Environ. Pollut. 305, 119258. https://doi.org/10.1016/j.envpol.2022.119258.

Ferreira, I., Venâncio, C., Lopes, I., Oliveira, M., 2019. Nanoplastics and marine organisms: what has been studied? Environ. Toxicol. Pharmacol. 67 (January), 1–7. https://doi.org/10.1016/j.etap.2019.01.006.

Foroozandeh, P., Aziz, A.A., 2018. Insight into cellular uptake and intracellular trafficking of nanoparticles. Nanoscale Res. Lett. 13, 339. https://doi.org/10.1186/s11671-018-2728-6.

Gaudioso, Á., Silva, T.P., Dolores Ledesma, M., 2022. Models to study basic and applied aspects of lysosomal storage disorders. Adv. Drug Deliv. Rev. 190, 114532. https://doi.org/10.1016/j.addr.2022.114532.

Gustafson, H.H., Holt-Casper, D., Grainger, D.W., Ghandehari, H., 2015. Nanoparticle uptake: the phagocyte problem. Nano Today 10 (4), 487–510. https://doi.org/10.1016/j.nantod.2015.06.006.

He, W., Liu, S., Zhang, W., Yi, K., Zhang, C., Pang, H., Huang, D., Huang, J., Li, X., 2023. Recent advances on microplastic aging: Identification, mechanism, influence factors, and additives release. Sci. Total Environ. 889, 164035. https://doi.org/10.1016/j.scitotenv.2023.164035.

Hu, M., Palić, D., 2020. Micro- and nano-plastics activation of oxidative and inflammatory adverse outcome pathways. Redox Biol. 37, 101620. https://doi.org/10.1016/j.redox.2020.101620.

Jeon, S., Lee, D.K., Jeong, J., Yang, S.I., Kim, J.S., Kim, J., Cho, W.S., 2021. The reactive oxygen species as pathogenic factors of fragmented microplastics to macrophages. Environ. Pollut. 281, 117006. https://doi.org/10.1016/j.envpol.2021.117006.

Karami, A., 2017. Gaps in aquatic toxicological studies of microplastics. Chemosphere 184, 841–848. https://doi.org/10.1016/j.chemosphere.2017.06.048.

Kataoka, C., Kashiwada, S., 2021. Ecological risks due to immunotoxicological effects on aquatic organisms. Int. J. Mol. Sci. 22 (15). https://doi.org/10.3390/ijms22158305.

Katsumiti, A., Losada-Carrillo, M.P., Barros, M., Cajaraville, M.P., 2021. Polystyrene nanoplastics and microplastics can act as Trojan horse carriers of benzo(a)pyrene to mussel hemocytes in vitro. Sci. Rep. 11 (1). https://doi.org/10.1038/s41598-021-01938-4.

Katsumiti, A., Tomovska, R., Cajaraville, M.P., 2017. Intracellular localization and toxicity of graphene oxide and reduced graphene oxide nanoplatelets to mussel hemocytes in vitro. Aquat. Toxicol. 188, 138–147. https://doi.org/10.1016/j.aquatox.2017.04.016.

Le Foll, F., Rioult, D., Boussa, S., Pasquier, J., Dagher, Z., Leboulenger, F., 2010. Characterisation of Mytilus edulis hemocyte subpopulations by single cell time-lapse motility imaging. Fish. Shellfish Immunol. 28 (2), 372–386. https://doi.org/10.1016/j.fsi.2009.11.011.

Liu, L., Du, R., Niu, L., Li, P., Li, Z.H., 2024. A latest review on micro- and nanoplastics in the aquatic environment: the comparative impact of size on environmental behavior and toxic effect. Bull. Environ. Contam. Toxicol. 112 (2). https://doi.org/10.1007/s00128-024-03865-2.

Lu, Q., Zhou, Y., Sui, Q., Zhou, Y., 2023. Mechanism and characterization of microplastic aging process: a review. Front. Environ. Sci. Eng. 17 (8). https://doi.org/10.1007/s11783-023-1700-6.

Lunov, O., Syrovets, T., Loos, C., Nienhaus, G.U., Mailänder, V., Landfester, K., Rouis, M., Simmet, T., 2011. Amino-functionalized polystyrene nanoparticles activate the NLRP3 inflammasome in human macrophages. ACS Nano 5 (12), 9648–9657. https://doi.org/10.1021/nn203596e.

Luo, Y., Wang, W.X., 2022. Immune responses of oyster hemocyte subpopulations to in vitro and in vivo zinc exposure. Aquat. Toxicol. 242, 106022. https://doi.org/10.1016/j.aquatox.2021.106022.

Magrì, D., Sánchez-Moreno, P., Caputo, G., Gatto, F., Veronesi, M., Bardi, G., Catelani, T., Guarnieri, D., Athanassiou, A., Pompa, P.P., Fragouli, D., 2018. Laser ablation as a versatile tool to mimic polyethylene terephthalate nanoplastic pollutants: characterization and toxicology assessment. ACS Nano 12 (8), 7690–7700. https://doi.org/10.1021/acsnano.8b01331.

Nel, A.E., Mädler, L., Velegol, D., Xia, T., Hoek, E.M.V., Somasundaran, P., Klaessig, F., Castranova, V., Thompson, M., 2009. Understanding biophysicochemical interactions at the nano-bio interface. Nat. Mater. 8 (7), 543–557. https://doi.org/10.1038/nmat2442.

Oberle, C., Huai, J., Reinheckel, T., Tacke, M., Rassner, M., Ekert, P.G., Buellesbach, J., Borner, C., 2010. Lysosomal membrane permeabilization and cathepsin release is a Bax/Bak-dependent, amplifying event of apoptosis in fibroblasts and monocytes. Cell Death Differ. 17 (7), 1167–1178. https://doi.org/10.1038/cdd.2009.214.

Olabarrieta, I., L'azou, B., Yuric, S., Cambar, J., Cajaraville, M.P., Zelularra, B., Laborategia, H., Eta, Z., Zelulen, A., Saila, D., Fakultatea, Z., 2001. In vitro effects of cadmium on two different animal cell models. Toxicol. Vitr. 15, 511–517. https://doi.org/10.1016/S0887-2333(01)00056-X.

Pequeno, J., Antunes, J., Dhimmer, V., Bessa, F., Sobral, P., 2021. Microplastics in marine and estuarine species from the coast of Portugal. Front. Environ. Sci. 9. https://doi.org/10.3389/fenvs.2021.579127.

Prinz, N., Korez, Š., 2020. Understanding How Microplastics Affect Marine Biota on the Cellular Level Is Important for Assessing Ecosystem Function: A Review. In YOUMARES 9 - The Oceans: Our Research, Our Future. Springer International Publishing, pp. 101–120. https://doi.org/10.1007/978-3-030-20389-4_6.

Qu, X., Su, L., Li, H., Liang, M., Shi, H., 2018. Assessing the relationship between the abundance and properties of microplastics in water and in mussels. Sci. Total Environ. 621, 679–686. https://doi.org/10.1016/j.scitotenv.2017.11.284.

Revel, M., Roman, C., Châtel, A., 2021. Is cell culture a suitable tool for the evaluation of micro- and nanoplastics ecotoxicity? Ecotoxicology 30 (3), 421–430. https://doi.org/10.1007/s10646-021-02355-z.

Rinkevich, B., 2011. Cell cultures from marine invertebrates: new insights for capturing endless stemness. Mar. Biotechnol. 13 (3), 345–354. https://doi.org/10.1007/s10126-010-9354-3.

Roman, C., Mahé, P., Latchere, O., Catrouillet, C., Gigault, J., Métais, I., Châtel, A., 2023. Effect of size continuum from nanoplastics to microplastics on marine mussel Mytilus edulis: comparison in vitro/in vivo exposure scenarios. Comp. Biochem. Physiol. Part C Toxicol. Pharmacol. 264, 109512. https://doi.org/10.1016/j.cbpc.2022.109512.

Rosales, C., Uribe-Querol, E., 2017. Phagocytosis: a fundamental process in immunity. BioMed. Res. Int. 2017. https://doi.org/10.1155/2017/9042851.

Salvati, A., Åberg, C., dos Santos, T., Varela, J., Pinto, P., Lynch, I., Dawson, K.A., 2011. Experimental and theoretical comparison of intracellular import of polymeric nanoparticles and small molecules: toward models of uptake kinetics. Nanomed.

Nanotechnol. Biol. Med. 7 (6), 818–826. https://doi.org/10.1016/j.nano.2011.03.005.
Sendra, M., Carrasco-Braganza, M.I., Yeste, P.M., Vila, M., Blasco, J., 2020. Immunotoxicity of polystyrene nanoplastics in different hemocyte subpopulations of Mytilus galloprovincialis. Sci. Rep. 10 (1), 1–14. https://doi.org/10.1038/s41598-020-65596-8.
Sharifinia, M., Bahmanbeigloo, Z.A., Keshavarzifard, M., Khanjani, M.H., Lyons, B.P., 2020. Microplastic pollution as a grand challenge in marine research: a closer look at their adverse impacts on the immune and reproductive systems. Ecotoxicol. Environ. Saf. 204. https://doi.org/10.1016/j.ecoenv.2020.111109.
Simmons, S.O., Fan, C.Y., Ramabhadran, R., 2009. Cellular stress response pathway system as a sentinel ensemble in toxicological screening. Toxicol. Sci. 111 (2), 202–225. https://doi.org/10.1093/toxsci/kfp140.
Sioen, M., Vercauteren, M., Blust, R., Town, R.M., Janssen, C., Asselman, J., 2024. Impact of weathered and virgin polyethylene terephthalate (PET) micro- and nanoplastics on growth dynamics and the production of extracellular polymeric substances (EPS) of microalgae. Sci. Total Environ. 953. https://doi.org/10.1016/j.scitotenv.2024.176074.
Stern, S.T., Adiseshaiah, P.P., Crist, R.M., 2012. Autophagy and lysosomal dysfunction as emerging mechanisms of nanomaterial toxicity. Part. Fibre Toxicol. 9. https://doi.org/10.1186/1743-8977-9-20.
Tanguy, M., Gauthier-Clerc, S., Pellerin, J., Danger, J.M., Siah, A., 2018. The immune response of Mytilus edulis hemocytes exposed to Vibrio splendidus LGP32 strain: a transcriptomic attempt at identifying molecular actors. Fish. Shellfish Immunol. 74, 268–280. https://doi.org/10.1016/j.fsi.2017.12.038.
Thibodeau, M.S., Giardina, C., Knecht, D.A., Helble, J., Hubbard, A.K., 2004. Silica-induced apoptosis in mouse alveolar macrophages is initiated by lysosomal enzyme activity. Toxicol. Sci. 80 (1), 34–48. https://doi.org/10.1093/toxsci/kfh121.
Völkl, M., Jérôme, V., Weig, A., Jasinski, J., Meides, N., Strohriegl, P., Scheibel, T., Freitag, R., 2022. Pristine and artificially-aged polystyrene microplastic particles differ in regard to cellular response. J. Hazard. Mater. 435. https://doi.org/10.1016/j.jhazmat.2022.128955.
von der Esch, E., Lanzinger, M., Kohles, A.J., Schwaferts, C., Weisser, J., Hofmann, T., Glas, K., Elsner, M., Ivleva, N.P., 2020. Simple Generation of Suspensible Secondary Microplastic Reference Particles via Ultrasound Treatment. Front. Chem. 8. https://doi.org/10.3389/fchem.2020.00169.
Wang, F., Bexiga, M.G., Anguissola, S., Boya, P., Simpson, J.C., Salvati, A., Dawson, K.A., 2013. Time resolved study of cell death mechanisms induced by amine-modified polystyrene nanoparticles. Nanoscale 5 (22), 10868–10876. https://doi.org/10.1039/c3nr03249c.
Wang, T., Huang, X., Jiang, X., Hu, M., Huang, W., Wang, Y., 2019. Differential in vivo hemocyte responses to nano titanium dioxide in mussels: effects of particle size. Aquat. Toxicol. 212, 28–36. https://doi.org/10.1016/j.aquatox.2019.04.012.
Xia, T., Kovochich, M., Liong, M., Zink, J.I., Nel, A.E., 2008. Cationic polystyrene nanosphere toxicity depends on cell-specific endocytic and mitochondrial injury pathways. ACS Nano 2 (1), 85–96. https://doi.org/10.1021/nn700256c.
Yang, M., Wang, W.X., 2022. Differential cascading cellular and subcellular toxicity induced by two sizes of nanoplastics. Sci. Total Environ. 829. https://doi.org/10.1016/j.scitotenv.2022.154593.
Yoon, J., Kim, K., Park, H., Choi, C., Jang, S., Park, Y., 2015. Label-free characterization of white blood cells by measuring 3D refractive index maps. Biomed. Opt. Express 6 (10), 3865–3875. https://doi.org/10.1364/boe.6.003865.